Molecular-Dynamics and First-Principles Calculations of Raman Spectra and Molecular and Electronic Structure of Hydrogen Clusters in Hydrogen Clathrate Hydrate

ARTICLE *in* THE JOURNAL OF PHYSICAL CHEMISTRY C · DECEMBER 2010

Impact Factor: 4.77 · DOI: 10.1021/jp106788u

4 AUTHORS:

Jianwei Wang
Louisiana State University
73 PUBLICATIONS **1,191** CITATIONS
SEE PROFILE

Udo Becker
University of Michigan
916 PUBLICATIONS **12,580** CITATIONS
SEE PROFILE

Hailong Lu
Peking University
55 PUBLICATIONS **537** CITATIONS
SEE PROFILE

John A. Ripmeester
National Research Council Canada
713 PUBLICATIONS **15,630** CITATIONS
SEE PROFILE

Molecular-Dynamics and First-Principles Calculations of Raman Spectra and Molecular and Electronic Structure of Hydrogen Clusters in Hydrogen Clathrate Hydrate

Jianwei Wang,*,† Hailong Lu,‡ John A. Ripmeester,‡ and Udo Becker†

Department of Geological Sciences, University of Michigan, 1100 North University Ave., Ann Arbor, Michigan, 48109, United States, and Steacie Institute for Molecular Sciences, National Research Council Canada, 100 Sussex Drive, Ottawa, Ontario K1A 0R6, Canada

Received: July 21, 2010; Revised Manuscript Received: October 25, 2010

Molecular-dynamics simulations and first-principles calculations are employed to understand vibrational spectroscopy and molecular and electronic structure of the encaged hydrogen molecules in hydrogen clathrate hydrate. The molecular-dynamics simulations, using empirical potentials, are performed to generate collections of the clathrate water cages with different hydrogen occupancies. The first-principles calculations, using Density Functional Theory with B3LYP hybrid density functionals for exchange and correlation, are carried out to optimize the structures and to calculate the Raman shift and activity of the stretching mode of the encaged hydrogen molecules. The Raman spectra are computed by a weighted moving average over a number of different structural configurations for different hydrogen occupancies. The results show that experimentally observed Raman peaks around 4120−4125 cm^{-1} are from small cages with single H_2 occupancy and peaks around 4125−4150 cm^{-1} from those in the large cages with one to four H_2 molecules. The Raman peaks of hydrogen molecules in the doubly occupied small cages are expected to be around or above the gas phase frequency 4155 cm^{-1}. Molecular structural analysis shows that the single hydrogen molecule in the small cages and single to quadruple hydrogen molecules in the large cage are encaged in loose cages, while double hydrogen molecules in the small cage are confined in a tight cage. Normal-mode analysis shows that there is limited vibrational coupling for H_2 molecules in doubly to quadruply occupied large cages while a strong vibrational coupling is observed in the doubly occupied small cage. The isovalue maps of total electron density and electrostatic potential suggest significant electron sharing between hydrogen molecules and water molecules, and important interaction between hydrogen and water oxygen atoms for confining the hydrogen clusters. The results help explain experimentally observed Raman spectra of hydrogen clathrates and provide new insights into the confinement effect by the water host framework on vibrational, molecular, and electronic properties of hydrogen molecules in the cages of clathrate hydrates.

Introduction

Hydrogen clathrate hydrates are inclusion compounds with hydrogen molecules occupying cages that are formed by hydrogen-bonded water molecules. The local hydrogen-bonding network of hydrogen clathrates is similar to that in ice Ih. The structures have been determined as being of clathrate hydrate type II.[1] Due to their comparably high hydrogen-storage capacity (up to ∼5 wt %), hydrogen hydrates have a great potential to be used as a H_2 storage medium for clean energy technology.[1−5] Unlike any other materials for hydrogen storage, hydrogen clathrate has only water and hydrogen molecules in the structure, and after combustion, hydrogen clathrate only releases water, so it is environmentally friendly. However, hydrogen clathrates are not well understood, and controversies remain about the H_2 cage occupancy and the characterization of hydrogen-containing hydrates in general.[5] This lack of understanding prevents further research and development of the hydrogen clathrate hydrates for energy applications since the H_2 cage occupancy directly affects the hydrogen storage capacity.

Experimental results and theoretical calculations provide a consistent picture on the occupancy of the large cages, each of which can accommodate up to four H_2 (or D_2) molecules in pure H_2 (or D_2) clathrate hydrate.[1,2,6−8] In contrast, conflicting explanations of experimental results have been reported regarding maximum H_2 occupancy in the small cages in both pure hydrogen hydrate[1,6] and binary tetrahydrofuran (THF or $(CH_2)_4O$)−hydrogen hydrates.[3,4,9] Inconclusive results have also been reported from different theoretical studies. Patchkovskii and Tse,[2] Inerbaev et al.,[10] and Sebastianelli et al.[11] proposed double occupancy, while Alavi et al.[7] and Papadimitriou et al.[12] suggested single occupancy. On incorporating quantum corrections into the empirical potential, Alavi et al.[7] carried out molecular-dynamics simulations and concluded that a number of different cage-occupancy configurations are close in configurational energy,[13] such that one may expect that, in a bulk sample, a number of these may in fact coexist. Indeed, recent experiments using Raman spectroscopy support a mixture of different hydrogen occupancies in the large cages.[14,15] However, uncertainty regarding the optimal hydrogen occupancy in the small cages remains. Although most of the recent experiments support single occupancy in the small cages,[3,14−16] it is not clear that hydrogen clathrate with hydrogen doubly occupied small cages is possible as previously reported in a high-pressure experiment.[1] There is also some uncertainty about the Raman frequency range of hydrogen molecules in the doubly occupied small cages. This situation prevents appropriate Raman char-

* To whom correspondence should be addressed, jwwang@umich.edu.
† University of Michigan.
‡ National Research Council Canada.

10.1021/jp106788u
Published on Web 11/22/2010

acterization of hydrogen clathrates and their research and applications.

Molecular modeling of the vibrational spectrum of the encaged H_2 molecules would provide the theoretical basis and insights into these controversies. In addition, the fact that multiple H_2 molecules with very short H_2-H_2 distances exist inside the cages suggests a significant confinement effect and unconventional interactions. However, the nature of the forces that keep hydrogen molecules entrapped and that stabilize the clathrates remains elusive. It is also not clear as to what extent quantum effects control the occupancies and stabilities of the H_2 clusters. As a result, theoretical investigations are needed to unravel the fundamental basis for hydrogen clustering in the clathrate cages.

In order to better understand the vibrational spectroscopy, the molecular and electronic structure, and the interactions between H_2 and H_2O molecules and among the H_2 clusters in the hydrogen clathrate, quantum-mechanical calculations on collections of isolated hydrogen-filled cages from pure H_2 clathrate are carried out. Raman spectra, the molecular structure of hydrogen and water, total electron-density isovalue maps, and electrostatic−potential isovalue surfaces are calculated. The results provide a theoretical view of what roles the intermolecular electron sharing, intermolecular vibrational coupling, and electrostatic potentials from water play in confining highly condensed H_2 clusters in the clathrate. Raman shifts and vibrational coupling of the H_2 clusters in clathrate cages will also provide important insights on different confinement effects of enclathrating H_2 molecules with respect to pressurizing the molecules in condensed-phase hydrogen or hydrogen-filled ice phases.

Methods

Hydrogen clathrate has a type II hydrate structure (Figure 1a) with a space group *Fd3m* and two types of cages: the large one (L) is a hexakaidecahedron ($5^{12}6^4$) with 28 H_2O (Figure 1b) and the small one (S) is a pentagonal dodecahedron (5^{12}) with 20 H_2O (Figure 1c). The crystal structural unit cell has 136 H_2O, with 16 S and 8 L cages. In the calculations, the initial structure of the H_2O framework is based on a refined sII structure as obtained from X-ray single crystal diffraction,[17] and the original guest molecules are replaced with H_2 molecules near the centers of the S and L cages. The initial positions of water hydrogen atoms are randomly chosen while keeping each water molecules with two hydrogen atoms. In order to eliminate net dipole moment for the system with such a configuration, empirical-potential energy minimizations and molecular dynamics simulations at constant volume and finite temperature (NVT) are performed on a supercell with $2 \times 2 \times 2$ unit cells of sII structure, using the GROMACS package,[18] the SPC/E model for H_2O,[19,20] and a simple point charge model for H_2.[7,21] During the simulations, the water oxygen atoms are fixed. With this procedure, the net dipole moment for the system is reduced to a minimum. The NPT runs without fixing oxygen positions are then equilibrated for 500 ps at 150 K and 200 MPa, within the stability field of the hydrogen hydrate;[1] subsequently, the equilibrated supercell is quenched. Because calculations with acceptable accuracy using first-principles techniques for the simulation supercell with over 500 atoms are currently not feasible, each of the cages with filled hydrogen molecules is isolated from the supercell. (These cages are treated using a quantum-mechanical cluster approach in this study (see below)). The structures of the cages are then optimized with the same force fields by energy minimization. For the energy minimization, a steepest-descent algorithm is used. For the MD simulations, the time step is 0.5 fs. The cutoff distance for van der Waals' interaction is 1.0 nm. The fast particle-mesh Ewald method is used for the electrostatic interaction.[22] The time constant for temperature coupling is set at 0.1 ps and the time constant for pressure coupling is 1.0 ps. Temperature coupling is achieved by using a Nose−Hoover extended ensemble. The isotropic Parrinello−Rahman scheme is used in pressure coupling. LINCS, an algorithm that resets bonds to their correct lengths after an unconstrained update, is used in the MD simulations. For general information on MD simulations and applications, please refer to books about MD simulation methods[23,24] and our recent articles on MD applications.[25−32]

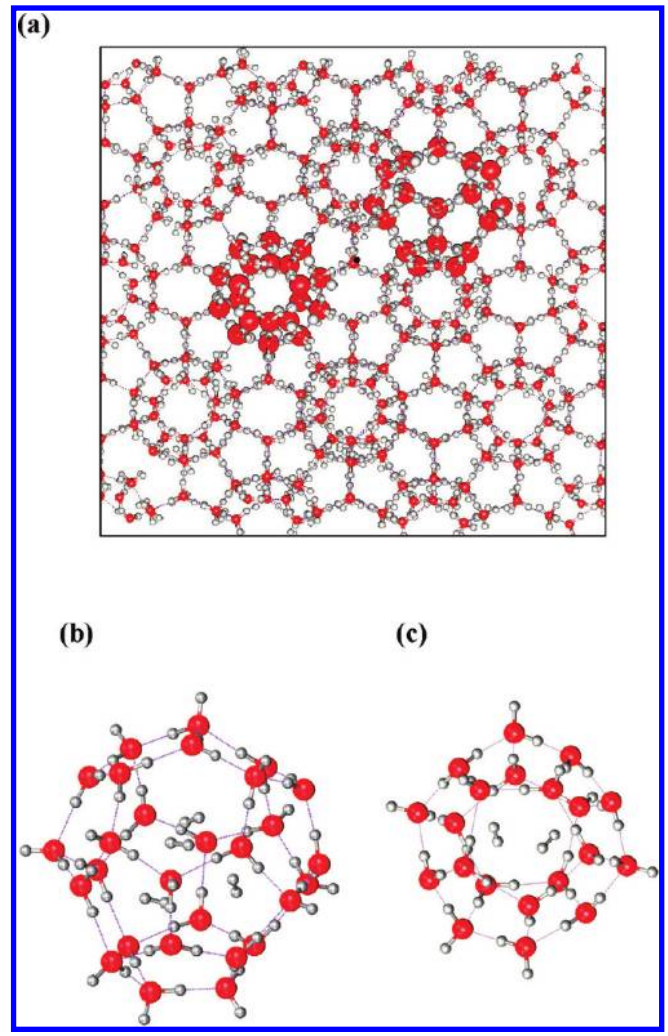

Figure 1. Structure of clathrate hydrate sII. Red balls are oxygen atoms, and light gray balls are hydrogen atoms. One large cage and one small cage are highlighted with larger balls. Dotted blue lines are hydrogen bonds. (a) Crystal structure of sII hydrate. (b) A larger cage with four encaged hydrogen molecules. (c) A small cage with two encaged hydrogen molecules.

The density functional theory (DFT) calculations are performed on the empirical potential optimized cages with a two-level ONIOM model,[33] which is implemented in the GAUSSIAN 03 package.[34,35] In this model, atoms selected for the high-level calculation have a larger basis set than those for the low level. In this study, the high level includes only the H_2 molecules and the low level includes the H_2O molecules. Closed-shell spin-restricted DFT calculations are performed with B3LYP hybrid density functional for exchange and correlation,[36] 6-31++G(2d,2p) basis set for the high level and 3-21+G(d,p) for the

low level. Both the H_2O framework and H_2 clusters are kept flexible, and no constraints are applied to fix atomic positions or molecular orientations during the structural optimizations. This flexibility allows more accurate calculations of the Raman spectrum. However, the average size of each type of cages will also change and the effect on the properties of the hydrogen molecules will be discussed. Convergence is tested against criteria for the maximum force component, root-mean-square force, and maximum step component. The threshold for the maximum force is 0.00045 au, root-mean-square force 0.0003 au, and maximum displacement 0.0018 au. For each of the occupancies in the L cages (L^0−L^4), 11 cages are successfully optimized. For the S cages, 19 S^2, 29 S^1, and 29 S^0 cages are successfully optimized. These cages are collections of the structural configurations of L and S cages with different H_2 occupancies.

With the optimized structures, Raman vibrational frequencies are computed by determining the second derivatives of the energy with respect to the Cartesian coordinates and then transforming to mass-weighted coordinates.[34] The vibrational analysis is achieved by diagonalizing the vibrational matrix

$$H_{ij} = \frac{1}{\sqrt{m_i m_j}} \frac{\partial^2 E_{\text{total}}}{\partial q_i \partial q_j} \quad (1)$$

$$H_{ij} U_k = \lambda_k U_k \quad (2)$$

$$\lambda_k = (2\pi v_k)^2 \quad (3)$$

where H_{ij} is the vibrational matrix, m_i is the mass of the ith atom, q_i is the displacement of this atom in the x, y, and z directions, E_{total} is the total energy of the system, U_k is the kth vibrational mode, and the eigenvalue λ_k is related to the vibrational frequencies by eq 3. This results in $3N - 6$ vibrational frequencies with three translational frequencies and three rotational frequencies for a system with N atoms. All translational frequencies and rotational frequencies are close to zero or less than 10 cm^{-1}. After projecting out translational and rotational modes, any imaginary frequency was checked and the related mode was visualized before the calculated frequencies were used for computing the average Raman spectrum. If an imaginary frequency is present in the frequency output, it has to be less than a few tens of wavenumbers (e.g., 50 cm^{-1}), which is usually around the upper limit of a translational mode using numerical integration.[34] If a calculation results in one or more large imaginary frequencies (over 50 cm^{-1}), reoptimization with tight criteria was applied. Out of 92 calculations used for computing the averaged Raman spectra, there are three imaginary frequencies above 50 cm^{-1} (from 65 to 95 cm^{-1}). These three modes do not involve major structural changes. Considering that the systems are relatively large and weakly bonded by hydrogen bonds and van der Waals interactions, a small number of imaginary modes indicates that the optimizations have converged well enough for understanding the trend of vibrational properties of hydrogen in the hydrate, although better frequency calculations to eliminate any imaginary frequencies would be possible with significant additional computational effort.

Similar calculations using different basis sets and SPC/E empirical potentials for the low-level H_2O molecules have also been carried out. The absolute values of the Raman frequencies and differences between Raman peaks are noticeably dependent on the basis sets or empirical potentials used for the low-level species. However, for all calculations, the relative Raman peaks shift directions (blue shift or red shift with respect to each other) are consistent. The basis set used for the results reported in this study reproduces the experimental Raman spectra well with affordable computational cost. Raman spectra in the H_2 stretching region are computed as a moving average of calculated Raman frequencies, weighted with Raman activities, and normalized using the stoichiometric numbers of the cages in the compound. Although the numbers of the structural configurations are relatively small, statistically meaningful Raman spectra are obtained as discussed in the next sections. Electron density and electrostatic potential surface maps are generated from the optimized self-consistent field calculations.

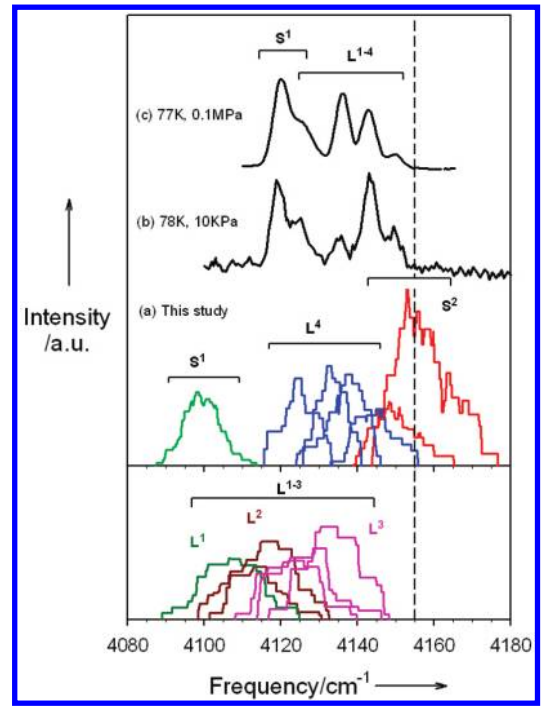

Figure 2. Raman spectra of hydrogen molecules in hydrogen clathrate hydrate. (a) Calculated spectra from quantum-mechanical calculations. The spectra are plotted as moving averages (the window size for averaging, 4 cm^{-1}). The calculated frequencies are scaled by a factor of 0.9367, the ratio between 4155 cm^{-1} of free H_2 gas and 4436 cm^{-1} of the calculated H−H stretching frequency of free isolated single H_2. Experiments by (b) Mao et al. (2002) and (c) Strobel et al. (2007). S^1, singly occupied small cage; S^2, doubly occupied small cage; L^1, L^2, L^3, and L^4, singly, doubly, triply, and quadruply occupied large cages. The vertical dashed line indicates 4155 cm^{-1} for free H_2 gas.

Results and Discussion

Raman Spectra of the Encaged Hydrogen Molecules. The calculated Raman spectra are shown in Figure 2a, along with two experimental results from the literature (spectra b and c in Figure 2).[1,37] A summary of the calculated spectra has been reported.[38] Details of explanations and discussions of the spectra are provided here along with some basic understanding for completeness. The calculated frequencies are scaled by a scaling factor because of well-documented systematic errors of the method.[39,40] The scaling factor for the methods employed in this study is estimated to be 0.9367, the ratio between 4155 cm^{-1} of observed free H_2 gas and 4436 cm^{-1} of the calculated H−H stretching frequency of free isolated single H_2. In the calculated spectra (Figure 2a), the lowest frequency peak around 4100 cm^{-1} is from H_2 in the S^1 cages. The four peaks from 4125 to 4145

cm^{-1} are from the L^4 cages. Two peaks from 4150 and 4157 cm^{-1} are from the S^2 cages. Peaks from 4100 to 4145 cm^{-1} are from the L^1, L^2, and L^3 cages. For the two experimental spectra shown in Figure 2b,c, the shapes and relative intensities vary significantly, although both of them were taken on samples of pure hydrogen hydrate.[1,37] However, the peak positions are, in general, consistent between the two experiments (Figure 2b,c).[1,37] The low-frequency end around 4120−4125 cm^{-1} of the experimental spectra is assigned to H_2 in the S^1 cages and the high-frequency end around 4125−4150 cm^{-1} to H_2 in the L cage (Figure 2), consistent with recent Raman spectroscopic studies of hydrogen clathrate.[14,15] However, overlap between S^1 and L^{1-4} peaks may occur as suggested by the calculations (Figure 2a). This assignment is also consistent with assigning Raman peaks between 4120 and 4125 cm^{-1} to the H_2 singly occupied small cages in THF hydrogen clathrate.[37]

Our calculated spectra are in qualitative agreement with the experimental observations in terms of relative peak positions and all the peaks from the S^1 and L^{1-4} cages are red-shifted with respect to 4155 cm^{-1} of H_2 in the low-density gas phase. Absolute values of the frequencies are, however, underestimated by ∼20 cm^{-1} for S^1 and ∼15−5 cm^{-1} for L^{1-4}. The underestimations may originate from the isolation of the cages from the crystal, which causes the distances between guest gas and water molecules to be reduced because of neglecting intercage hydrogen bonding (more discussion later). The discrepancy between observations and the calculations may also arise from the limitations of the DFT method from its inaccuracy in describing weak dispersive intermolecular interactions and the effects from the static calculations at 0 K (e.g., the athermal limit). Ab initio calculations at the MP2 level or quantum Monte Carlo methods might provide a better description of the dispersive interactions of the systems. It is also noteworthy to mention that cage-occupancy-induced Raman-peak splittings cannot account for all features in the experimental Raman spectra. Incomplete reaction, sample inhomogeneity, and multiple peaks due to a mixture of H_2 molecules at different rotational states (e.g., para-H_2 and ortho-H_2) at finite temperature contribute significant complications and variations of the observed Raman spectra. The quantum nature of the rotational states of the hydrogen molecules cannot be incorporated in the static DFT calculations presented here. In addition, the calculated spectrum is relatively broader than the observed spectrum because there are only a limited number of configurations considered. Nevertheless, as a qualitative guide for the relative trend of the observed Raman spectra, the calculated spectra are sufficient to be used for interpreting experimental results.

As shown in Figure 2, the Raman frequencies for the S^2 cages are around 4150 and 4157 cm^{-1}, well separated from the S^1 and L^4 peaks. Considering the underestimates of the calculated frequencies of the encaged H_2, the Raman frequencies from the doubly occupied small cage (S^2) are expected to be around or above 4155 cm^{-1}, blue-shifted with respect to the gas phase hydrogen. The highest frequencies in the experimental spectra of pure hydrogen clathrates occur at ∼4150 cm^{-1}, suggesting that the characteristic peaks of S^2 are not present in the previous experiments.[1,14,15,37] A more recent experimental result showed that, in addition to the Raman peaks from 4120 to 4150 cm^{-1}, there are two additional Raman peaks at ∼4153 and ∼4159 cm^{-1} of the encaged hydrogen,[41] which are around or above 4155 cm^{-1} of the gas phase frequency. These two peaks can be interpreted by the presence of two hydrogen molecules in the S^2 cages.[41]

We also note that the fine structure in the low-frequency band (4120−4125 cm^{-1}) of the experimental spectra is time-dependent over a period of days to weeks if the sample is stored in liquid nitrogen, with the high-frequency shoulder around 4125 cm^{-1} becoming stronger with respect to the main peak around 4120 cm^{-1}, consistent with a recent study of hydrogen clathrate at low temperature.[14,15] This kind of behavior can be attributed to very slow ortho- to para-H_2 conversion, which involves a change of H_2 nuclear spins at lower temperature of samples made at higher temperature.

Raman Shift and Confinement Effect. The red shift in H_2 vibrational frequencies in hydrogen hydrate with respect to the gas phase observed in the experiments and predicted in our calculations is also observed for adsorbed hydrogen molecules at inorganic surfaces and for other gas molecular species in clathrate hydrate systems. For instance, H−H stretching is red-shifted by 60 cm^{-1} for H_2 molecules adsorbed in the cages of zeolites[42] and red-shifted by 31 cm^{-1} for those adsorbed at the internal surface of Vycor glass.[43] In CH_4 clathrate hydrate, C−H stretching is red-shifted by 14 and 4 cm^{-1} in the large and small cages, respectively.[44,45] At moderate pressure, a vibrational frequency decrease of a molecule, perturbed by its local environment, often indicates a softened vibrational mode and a stretched intramolecular bond from the equilibrium of the isolated molecule. The molecule sees a potential energy surface where an attractive interaction with host molecules or surfaces is dominant. This is formalized in the so-called loose-cage tight-cage model.[44,46] In hydrogen clathrate, H_2 vibrons in S^1 have the largest red shift in the spectra (Figure 2), indicating that the molecules are loosely confined in a highly attractive potential field with little intermolecular repulsion. In L^4, a smaller red shift implies that the four H_2 molecules are still loosely confined and the repulsive interactions play a small role to offset the attraction. The frequencies of H_2 in L^3, L^2, and L^1 are successively shifted to lower wavenumbers from L^4, indicating that the repulsive interactions gradually decrease. The vibrons in S^2, on the other hand, are actually blue-shifted, suggesting that the attractive interaction is balanced by repulsive interactions between two H_2 and between H_2 and H_2O in a tightly confined space. Such a blue shift of Raman frequency of an encaged molecule in clathrate is not uncommon. For instance, for encaged propane (C_3H_8) in sII hydrate, the Raman stretching frequency of the C−H in the large cage is blue-shifted by 7 cm^{-1}.[47] For CO_2 in the large cage of sI, a blue shift of 96 cm^{-1} was observed for the C−O stretching mode.[47] The blue shift for H_2 in S^2 indicates the two hydrogen molecules are confined in a tight cage and the repulsive interaction is dominated. The relative shift of Raman frequencies of an encaged molecule in clathrates with respect to its gas phase is sensitive to the local molecular environment inside the cage.

Vibrational Coupling of Encaged Hydrogen Molecules. Visualization of vibrational modes of the encaged hydrogen molecules reveals that there is a fundamental difference in intermolecular vibrational coupling between hydrogen molecules in S^2 and among those in L^{2-4}. For the H_2 molecules in L^{2-4}, the orientations of the H_2 molecules are geometrically frustrated since it is difficult to achieve energetically equivalent geometric positions or same site symmetry for the nonspherical H_2 molecules. There is very limited vibrational coupling, and each H_2 vibration is independent of the rest of the H_2 molecules. In contrast, for the two H_2 in S^2, a strong vibrational coupling is observed in the calculations. All Raman calculations of 19 S^2 cages, without exception, show that the mode around 4150 cm^{-1} originates from the out-of-phase vibration of the two H_2. The mode around 4157 cm^{-1} corresponds to the in-phase vibration.

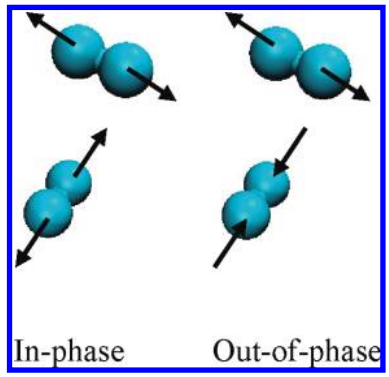

Figure 3. A schematic picture of in-phase and out-of-phase vibrational coupling of two diatomic molecules. The arrows are vibrational directions.

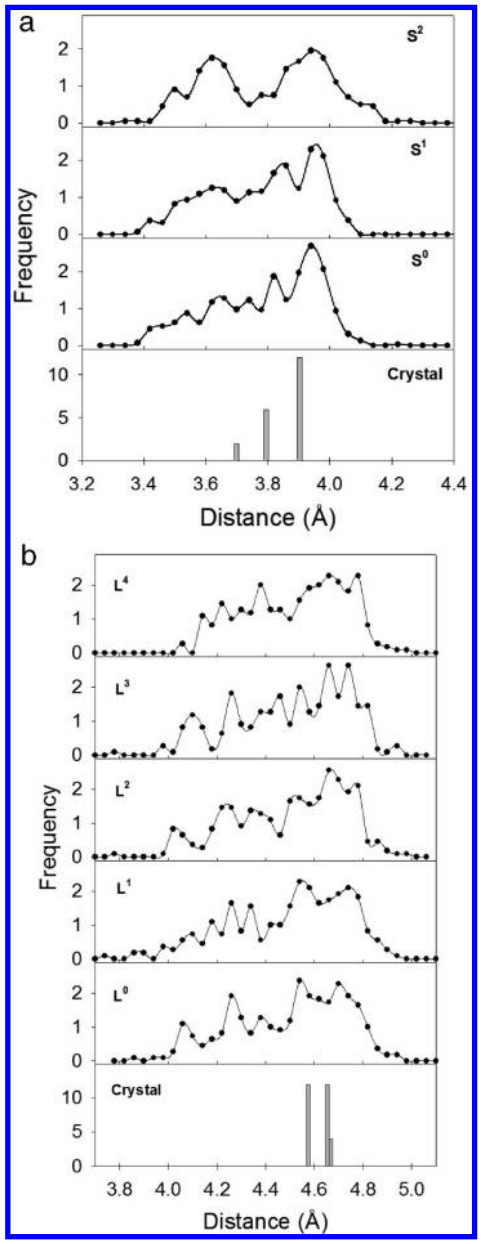

Figure 4. Statistical distributions of the distances from the center of the cages to the cage vertices of the water oxygen atoms: (a) the small cages and (b) the large cages. The vertical bars are the distances from the X-ray refined crystal structure.[1,52]

A schematic picture shows the in-phase and out-of-phase vibrational coupling in Figure 3.

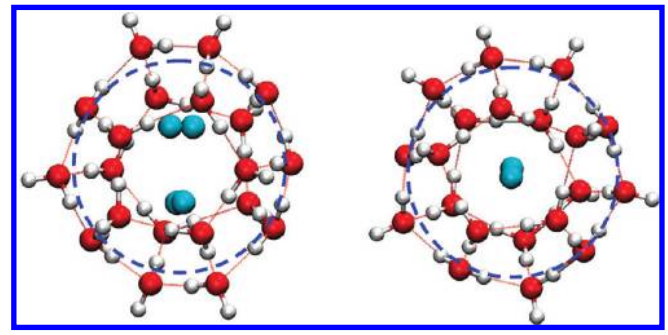

Figure 5. A comparison of the cage shape between a doubly occupied small cage (left) and a singly occupied small cage (right). The dashed circles are used as eye guides. The elongation of the doubly occupied cage is shown in the direction parallel to the line connecting the two H_2 molecules.

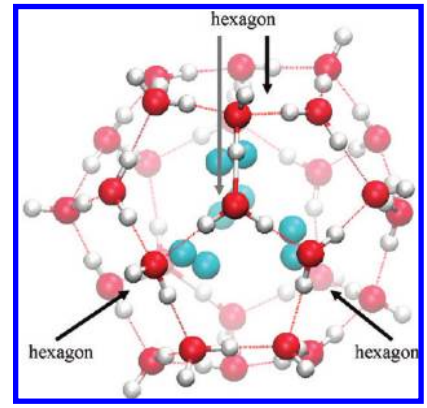

Figure 6. H_2 quadruply occupied large cage. The four H_2 molecules are close to the four hexagons of the $5^{12}6^4$ cage. A depth cueing view shows front and back molecules with different color saturation. The arrows point to the centers of the hexagons.

The vibrational coupling of two hydrogen molecules in the S^2 cage is surprising for a molecular cluster. In solid molecular hydrogen, in-phase coupled vibration is probed by Raman and out-of phase coupled vibration is probed by IR.[48] The difference between IR and Raman frequencies provides a measure of intermolecular coupling.[49] At zero pressure, the difference is 3 cm^{-1} (out-of-phase minus in-phase frequencies), and it increases with increasing pressure (about 10 cm^{-1} at 5 GPa).[48] The out-of-phase vibration has a higher frequency in solid molecular hydrogen.[48] Our calculations for hydrogen molecules in clathrate give a value of -7 cm^{-1} for the difference, with the in-phase vibration having a higher frequency. This result indicates a relatively strong coupling but with a completely different coupling scheme than the one in high-pressure solid H_2. The fundamental difference between the confinement effect and pressure effect is also evidenced by the fact that encapsulating hydrogen in clathrates mostly results in a stretching mode red shift while pressurizing solid hydrogen or hydrogen in ice always causes a blue shift.[48,50,51]

Structure of the Cages and Encaged H_2 Clusters. The geometries of the DFT-optimized cages are similar to the hexakaidecahedron (L cage) and pentagonal dodecahedron (S cage) from X-ray crystallographic structures. However, the cages are deviated from the experimental geometries. The reason for such deviation is that experimental cage geometries are highly symmetric and averaged structures over an ensemble of different configurations while only a small number of cages are used in the simulations without symmetry constraint. In addition, the isolated cages lack of intercage hydrogen bonding interaction, which contributes to the deviation from those in the crystal

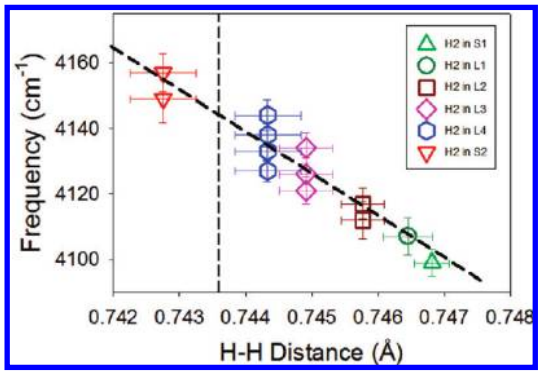

Figure 7. Correlation of the hydrogen intramolecular bond length with Raman vibrational stretching frequency. Up triangles are H_2 in S^1; down triangles are H_2 in S^2; circles are H_2 in L^1; squares are H_2 in L^2; diamonds are H_2 in L^3; hexagons are H_2 in L^4. The error bars are 1 standard deviation. The actual estimated errors are about 1 order of magnitude smaller. The vertical thin dashed line is the calculated H−H bond length of isolated H_2. The thick dashed line shows the overall trend of Raman frequency as a function of H−H distance.

phase. The deformations can be qualitatively described by comparing calculated and experimental distances between the center of the cage and the oxygen atoms at the vertices of the cage. As shown in Figure 4, distributions of the distances are shown for different cages with different cage occupancies. For the small cages (Figure 4a), the values range from 3.4 to 4.2 Å as compared with three distances at 3.69, 3.79, and 3.90 Å as determined in experiments. The coordinates of the reference crystal structure are taken from refined X-ray structural data for the hydrate sII structure[52] and the unit cell parameter (17.047 Å) is from the synthesized hydrogen clathrate.[1] As the hydrogen occupancy increases from S^0 and S^1 to S^2, the distribution is noticeably shifted to longer distances. For the large cages (Figure 4b), the distance is distributed from 4.0 to 4.9 Å, as compared with three distances at 4.56, 4.64, and 4.66 Å in the experimental crystal structure. As the hydrogen occupancy increases from L^0, L^1, L^2, L^3, to L^4, the distribution is also noticeably shifted to longer distances. By visualizing the optimized structures for both large and small cages, we do not observe significant geometric deviations from the crystal structure except for the small cages with two hydrogen molecules. For S^2, the cages are noticeably elongated along one direction, shown as two peaks around 3.62 and 3.96 Å in Figure 4a, which is parallel to the direction of connecting the centers-of-mass of the two hydrogen molecules. Therefore, the overall geometry for most of the optimized small cages (S^2) deviates from a perfect pentagonal dodecahedron. Figure 5 shows the S^2 cage deformation as compared with the S^1 cage. The estimated root-mean-square deviations of the oxygen atom coordinates of the optimized S^2 cages from the X-ray structure are 0.02 Å for the oxygen at 3.69 Å from the cage center, 0.01 Å for those at 3.79 Å, and 0.02 Å for those at 3.90 Å, with an average value of 0.02 Å.

Because isolated cage models are used, the intercage hydrogen bonding is neglected in the calculations, resulting in a systematic decrease in the size of the cages as compared with those in the crystal. The calculated average distances between the center of the cage and oxygen atoms at the vertices are smaller by 0.5−1.0% for the small cages and 1.8−2.3% for the large cages. This causes errors in the calculated Raman frequencies as compared with experimental observations as discussed before. The underestimations discussed previously on the Raman frequencies can be partially explained by the change of the cage

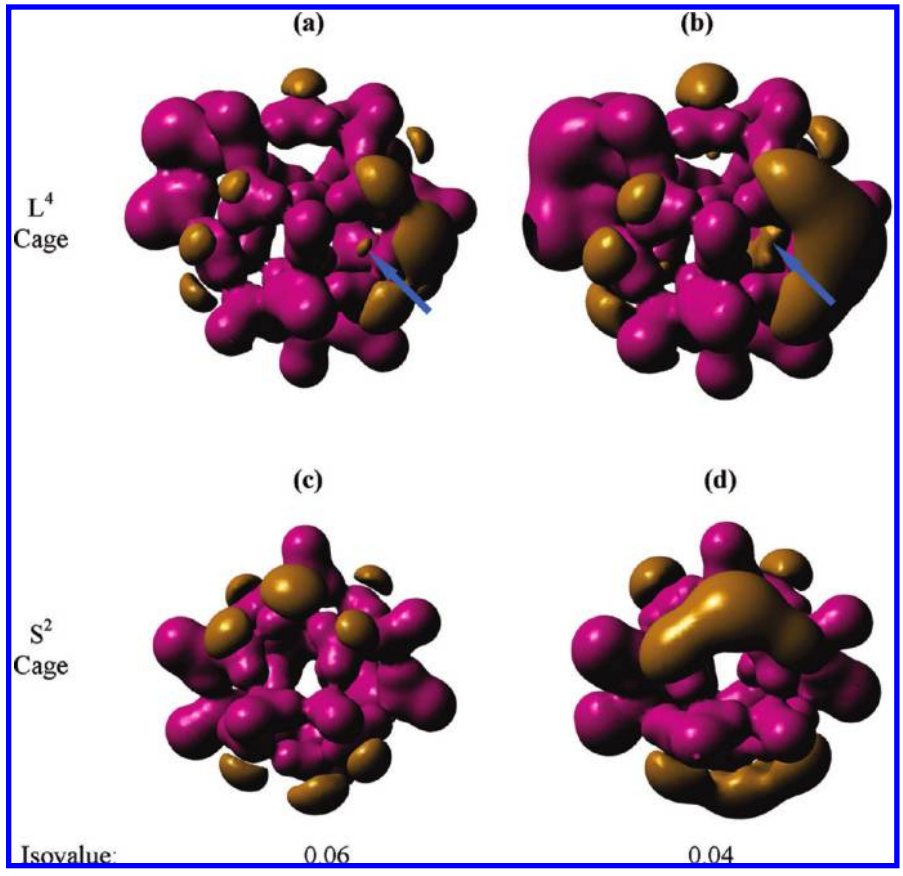

Figure 8. Electrostatic potential surfaces of the large (a and b) and small cage (c and d). Purple is for positive potentials and brown is for negative potentials. The isovalue is in atomic units at 0.06 (a and c) and 0.04 (b and d). The arrows point to negative potential regions within the cages.

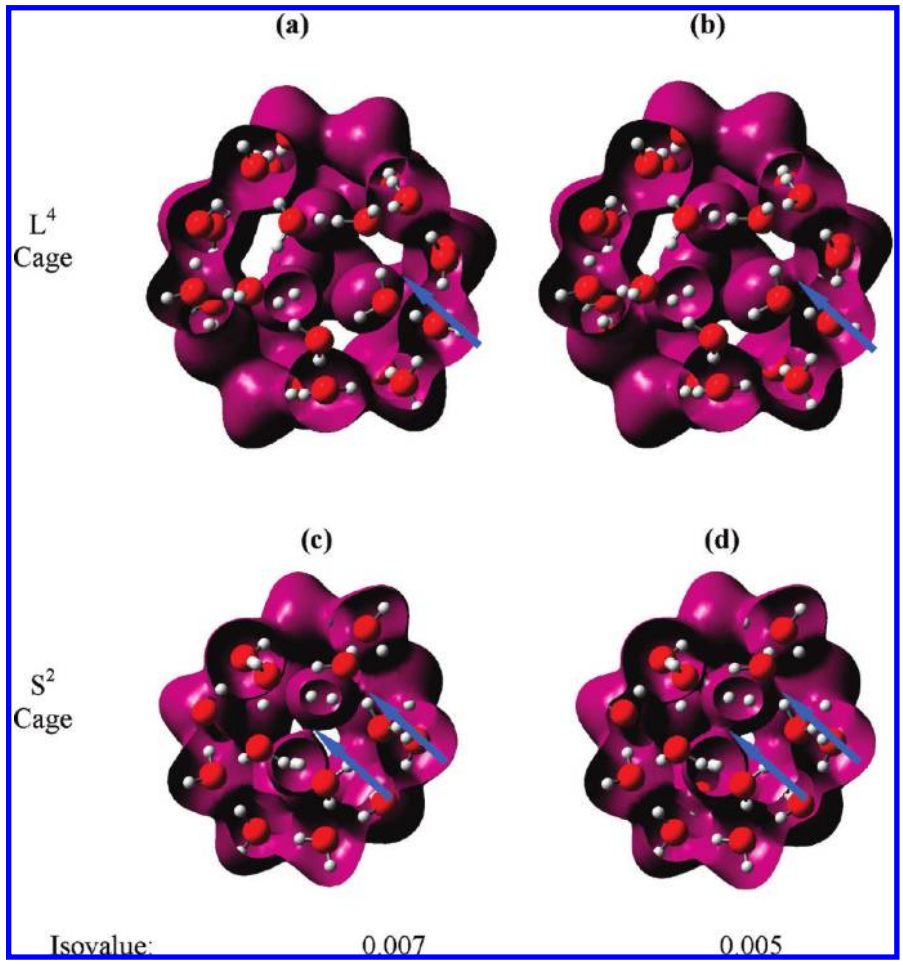

Figure 9. Electron density surfaces of the large (a and b) and small cages (c and d). Red balls are oxygen atoms and white balls are hydrogen atoms. The isovalue is in atomic units at 0.007 (a and c) and 0.005 (b and d). The arrows point to electron sharing regions within the cages.

size. Decrease in the distance between water oxygen atoms and encaged hydrogen molecules resulting from cage size reduction increases the negative potential on the hydrogen molecules from the lone pair region of the water oxygen atoms. This can cause the H_2 molecules to be in a more attractive potential field and results in smaller Raman frequencies. This is evident from the fact that the underestimation is less (5 cm^{-1}) for the fully occupied L^4 cage and more (15 cm^{-1}) for L^1, where larger underestimation is observed for the cage with greater cage size decrease. However, because the models and methods are consistent throughout the calculations for different types of cages with different occupancies, the trends and relative differences among Raman frequencies of different cages and occupancies are expected to be reliable even if the absolute values are only qualitative.

Structural analysis from our ab initio calculations shows that the H_2 molecules are highly condensed in S^2 and L^4 cages, consistent with previous experimental results and theoretical calculations.[2,6,11] In L^4, four H_2 molecules in the large cage form a slightly distorted tetrahedron. Each of the H_2 molecules is located near a face of a hexagon formed by the host water framework (Figure 6). In L^3, the three hydrogen molecules in a large cage form a triangle. Most of the H_2 molecules are still near a hexagon formed by the host water framework but not as close as those in L^4 cages. For large cages with two H_2 molecules and one H_2 molecule, no apparent association with the hexagon is observed for hydrogen molecules inside the cages. For L^4 cages, the calculated average H_2-H_2 distance between the centers of mass is 2.94 ± 0.11 Å, which is in excellent agreement with 2.93 Å from a neutron diffraction study of D_2 clathrate,[6] and with 2.90−3.13 Å from a quantum-chemistry study of H_2 clathrate.[2] Our theoretical calculations are also in accord with the neutron diffraction result[6] that the four H_2 molecules in L^4 form a tetrahedron. It needs to be mentioned that this structural configuration is based on static calculations at the athermal limit. At higher temperatures, however, the thermal energy may partially or fully activate H_2 rotational and translational motions.[6] For S^2 cages, the calculated average H_2-H_2 distance is 2.51 ± 0.03 Å, in good agreement with a value of 2.57 Å from quantum diffusion Monte Carlo (DMC) calculations,[11] and 2.58 Å from a quantum-chemistry calculation.[2] The H_2 intramolecular bonds in L^{1-4} and S^1 are stretched from the calculated gas phase equilibrium value, from 0.7436 Å to 0.7443 Å in L^4, to 0.7449 Å in L^3, to 0.7458 Å in L^2, to 0.7465 Å in L^1, to 0.7468 Å in S^1 cages, or ∼0.1−0.4% longer in L^{4-1} and 0.4% longer in S^1 cages. The intramolecular bonds in S^2 are compressed to 0.7427 Å or 0.1% shorter. The vibrational frequency of the hydrogen-stretching mode correlates strongly with the hydrogen intramolecular bond length as shown in Figure 7. As the H−H bond length decreases, the frequencies increase linearly. Except for those in S^2, all the encaged hydrogen molecules are stretched with respect to the free molecules and the vibrational frequencies are red-shifted. This result is consistent with the argument discussed earlier that H_2 molecules are loosely trapped in S^1 and L^{4-1}, and two H_2 molecules are tightly confined in S^2. This is also consistent with a Raman peak assignment that H_2 vibrons in S^1 and L^{4-1} have lower frequencies than those in S^2 cages.[38]

Electrostatic Potential and Electron Density. The short intermolecular distances at 2.94 Å in L^4 and 2.51 Å in S^2 in the clathrate are a dramatic decrease from an intermolecular distance (3.78 Å) in solid H_2 at low temperature.[53] This is equivalent to a decrease of the intermolecular distances by ~22% and ~34% in L^4 and S^2 cages, respectively, or, corresponding volume compressions by 53% and 71%, indicating fundamentally different intrinsic intermolecular interactions in hydrogen clathrate as compared with those in solid H_2. Interactions between H_2 and an electrostatic potential field from water oxygen and interactions arising from electron sharing among H_2 molecules within the H_2 clusters are important for confining them in the cages.

The electrostatic-potential isovalue maps are shown in Figure 8. There are noticeable negative electrostatic potential regions inside the cage in L^4, near the O side of H_2O at an isovalue of 0.06 au (Figure 8a), and they become significant at an isovalue of 0.04 au (Figure 8b). The same trend for the electrostatic potential is also observed for S^1 and L^{1-3} cages. In contrast, negative potential regions are absent inside the S^2 cage (Figure 8c,d) at the same isovalues. These two isovalues are chosen to demonstrate the changes of electrostatic potential. The difference indicates that the electrostatic potential from O of H_2O contributes more to the attractive interaction of H_2 molecules in L^4 than in S^2. This attractive interaction in L^{1-4} and S^1 is also evidenced by the fact that the H_2 molecules are stretched and that the H_2 vibrons are not coupled with each other and significantly softened with respect to the vibrons of free H_2 molecules. The total electron density isovalue maps (Figure 9) show that the electron density surfaces in L^4 are connected between H_2 and H_2O but not between H_2 molecules at isovalues of 0.005 and 0.007 au (Figure 9a,b). The similar trend for the electron density is also observed for S^1 and L^{1-3} cages. While the surfaces in S^2 are noticeably connected between H_2 and H_2O and between two H_2 at an isovalue of 0.007 au, these connections become substantial at an isovalue of 0.005 au (Figure 9c,d). Although the shared electron density is small, the result indicates that electron sharing between the H_2 molecules in S^2 is more pronounced than in L^{4-2}, arising from the shorter intermolecular distance and stronger electronic interaction. As comparing electron density overlap in S^1 with S^2, and L^1 with L^4, more overlap is observed in S^2 than in S^1 and in L^4 than in L^{1-3}. A previous study shows that, in a structure II hydrate, a significant electron density overlap between guest molecule and host water electron densities indicates instability for the hydrate.[54] Such significant overlap is not evident for S^{1-2} and L^{1-4} occupancies (Figure 9). Accurate thermodynamic stability assessment of different occupancies in the hydrate needs free energy calculation.

In summary, by combining quantum-mechanical calculations with classical molecular-dynamics simulations, average structure and vibrational spectra of H_2 in hydrogen clathrate are obtained. The results show that the H_2 molecules in the large cages and singly occupied small cages are stretched and the vibrational mode is softened and uncoupled. In the doubly occupied small cages, the H_2 molecules are slightly compressed with the vibrational frequencies close or above that of the free gas. The very short intermolecular distance between the two H_2 in the small cages leads to strong vibrational coupling. The calculations suggest that doubly occupied small cages in the clathrate would be signaled by the presence of Raman peaks around or higher than 4155 cm^{-1}. Innovative experimental methods may provide an opportunity to test the theoretical prediction and to raise the hydrogen capacity from ~3.4 wt % for the H_2 hydrate with $S^1 + L^4$ occupancy configuration to ~5 wt % with $S^2 + L^4$ configuration. The present work also shows a way to model a configurationally sensitive system with a collection of structures for better statistical average, which alleviates artificial effects from models based on a single structure.

Acknowledgment. This research was supported in part by the National Science Foundation through TeraGrid resources provided by NCSA and NICS. We acknowledge the support by the National Science Foundation NIRT Grant (EAR-0403732).

References and Notes

(1) Mao, W. L.; Mao, H.-K.; Goncharov, A. F.; et al. *Science* **2002**, *297*, 2247–2249.
(2) Patchkovskii, S.; Tse, J. S. *Proc. Natl. Acad. Sci. U.S.A.* **2003**, *100*, 14645–14650.
(3) Lee, H.; Lee, J.-W.; Kim, D. Y.; et al. *Nature* **2005**, *434*, 743–746.
(4) Strobel, T. A.; Taylor, C. J.; Hester, K. C.; et al. *J. Phys. Chem. B* **2006**, *110*, 17121–17125.
(5) Struzhkin, V. V.; Militzer, B.; Mao, W. L.; et al. *Chem. Rev.* **2007**, *107*, 4133–4151.
(6) Lokshin, K. A.; Zhao, Y. S.; He, D. W.; et al. *Phys. Rev. Lett.* **2004**, *93*, 125503.
(7) Alavi, S.; Ripmeester, J. A.; Klug, D. D. *J. Chem. Phys.* **2005**, *123*, 024507.
(8) Sebastianelli, F.; Xu, M.; BaCic, Z. *J. Chem. Phys.* **2008**, *129*, 244706–244709.
(9) Ogata, K.; Hashimoto, S.; Sugahara, T.; et al. *Chem. Eng. Sci.* **2008**, *63*, 5714–5718.
(10) Inerbaev, T. M.; Belosludov, V. R.; Belosludov, R. V.; et al. *Comput. Mater. Sci.* **2006**, *36*, 229–233.
(11) Sebastianelli, F.; Xu, M. Z.; Elmatad, Y. S.; et al. *J. Phys. Chem. C* **2007**, *111*, 2497–2504.
(12) Papadimitriou, N. I.; Tsimpanogiannis, I. N.; Papaioannou, A. T.; et al. *J. Phys. Chem. C* **2008**, *112*, 10294–10302.
(13) Alavi, S.; Klug, D. D.; Ripmeester, J. A. *J. Chem. Phys.* **2008**, *128*, 064506.
(14) Giannasi, A.; Celli, M.; Ulivi, L.; et al. *J. Chem. Phys.* **2008**, *129*, 084705−084710.
(15) Strobel, T. A.; Sloan, E. D.; Koh, C. A. *J. Chem. Phys.* **2009**, *130*, 014506−014510.
(16) Florusse, L. J.; Peters, C. J.; Schoonman, J.; et al. *Science* **2004**, *306*, 469–471.
(17) Kirchner, M. T.; Boese, R.; Billups, W. E.; et al. *J. Am. Chem. Soc.* **2004**, *126*, 9407–9412.
(18) van der Spoel, D.; Lindahl, E.; Hess, B.; et al. *Gromacs user manual version 3.3*; University of Groningen, 2005; www.gromacs.org.
(19) Berendsen, H. J. C.; Postma, J. P. M.; van Gunsteren, W. F.; et al. Interaction models for water in relation to protein hydration. In *Intermolecular Forces*; Pullman, B. , Ed.; Riedel: Dordrecht, 1981; pp 331−342.
(20) Berendsen, H. J. C.; Grigera, J. R.; Straatsma, T. P. *J. Phys. Chem.* **1987**, *91*, 6269–6271.
(21) Silvera, I. F.; Goldman, V. V. *J. Chem. Phys.* **1978**, *69*, 4209–4213.
(22) Essmann, U.; Perera, L.; Berkowitz, M. L.; et al. *J. Chem. Phys.* **1995**, *103*, 8577–8593.
(23) Allen, M. P.; Tildesley, D. J. *Computer simulation of liquids*; Clarendon Press: Oxford., 1987.
(24) Frenkel, D.; Smit, B. *Understanding Molecular Simulation from algorithms to applications*; Academic Press: New York, 2002.
(25) Wang, J. W.; Kalinichev, A. G.; Kirkpatrick, R. J.; et al. *Chem. Mater.* **2001**, *13*, 145–150.
(26) Wang, J.; Kalinichev, A. G.; Amonette, J. E.; et al. *Am. Mineral.* **2003**, *88*, 398–409.
(27) Kirkpatrick, R. J.; Kalinichev, A. G.; Wang, J. W. *Mineral. Mag.* **2005**, *69*, 289–308.
(28) Kirkpatrick, R. J.; Kalinichev, A. G.; Wang, J. W.; et al. Molecular modeling of the vibrational spectra of interlayer and surface species of layered double hydroxides. In *Application of Vibrational Spectroscopy to Clay Minerals and Layered Double Hydroxides*; Kloprogge, J. T., Ed.; The Clay Mineral Society: Aurora, CO, 2005; Vol. 13; pp 239−285.
(29) Wang, J.; Kalinichev, A. G.; Kirkpatrick, R. J. *Geochim. Cosmochim. Acta* **2006**, *70*, 562–582.
(30) Wang, J.; Rustad, J. R.; Casey, W. H. *Inorg. Chem.* **2007**, *46*, 2962–2964.
(31) Kalinichev, A. G.; Wang, J. W.; Kirkpatrick, R. J. *Cem. Concr. Res.* **2007**, *37*, 337–347.

(32) Wang, J.; Kalinichev, A. G.; Kirkpatrick, R. J. *J. Phys. Chem. C* **2009**, *113*, 11077–11085.
(33) Vreven, T.; Morokuma, K. *J. Comput. Chem.* **2000**, *21*, 1419–1432.
(34) Frisch, M. J.; Trucks, G. W.; Schlegel, H. B.; et al. *Gaussian 03 online manual*; Gaussian, Inc.: Wallingford, CT, 2003.
(35) Foresman, J. B. *Exploring chemistry with electronic structure methods*, 2nd ed.; Gaussian, Inc.: Pittsburgh, PA, 1996.
(36) Becke, A. D. *J. Chem. Phys.* **1993**, *98*, 5648–5652.
(37) Strobel, T. A.; Koh, C. A.; Sloan, E. D. *Fluid Phase Equilib.* **2007**, *261*, 382–389.
(38) Wang, J.; Lu, H.; Ripmeester, J. A. *J. Am. Chem. Soc.* **2009**, *131*, 14132–14133.
(39) Merrick, J. P.; Moran, D.; Radom, L. *J. Phys. Chem. A* **2007**, *111*, 11683–11700.
(40) Wong, M. W. *Chem. Phys. Lett.* **1996**, *256*, 391–399.
(41) Lu, H.; Wang, J.; Liu, C.; et al. Manuscript in preparation.
(42) Kazansky, V. B.; Jentoft, F. C.; Karge, H. G. *J. Chem. Soc., Faraday Trans.* **1998**, *94*, 1347.
(43) Huber, T. E.; Huber, C. A. *Phys. Rev. Lett.* **1987**, *59*, 1120 LP–1123.
(44) Subramanian, S.; Sloan, E. D. *J. Phys. Chem. B* **2002**, *106*, 4348–4355.
(45) Greathouse, J. A.; Cygan, R. T.; Simmons, B. A. *J. Phys. Chem. B* **2006**, *110*, 6428–6431.
(46) Buckingham, A. D. *Proc. R. Soc. London, Ser. A* **1958**, *248*, 169.
(47) Sum, A. K.; Burruss, R. C.; Sloan, E. D. *J. Phys. Chem. B* **1997**, *101*, 7371–7377.
(48) Mao, H.-K.; Hemley, R. J. *Rev. Mod. Phys.* **1994**, *66*, 671.
(49) van Kranendonk, J. *Solid hydrogen*; Plenum: New York, 1983.
(50) Hirai, H.; Ohno, S.; Kawamura, T.; et al. *J. Phys. Chem. C* **2007**, *111*, 312–315.
(51) Machida, S.-i.; Hirai, H.; Kawamura, T.; et al. *J. Chem. Phys* **2008**, *129*, 224505–224505.
(52) Mak, T. C. W.; McMullan, R. K. *J. Chem. Phys.* **1965**, *42*, 2732–2737.
(53) Ishmaev, S. N.; Sadikov, I. P.; Chernyshev, A. A.; et al. *J. Exp. Theor. Phys.* **1983**, *84*, 394.
(54) Greathouse, J. A.; Cygan, R. T.; Bradshaw, R. W.; et al. *J. Phys. Chem. C* **2007**, *111*, 16787–16795.

JP106788U